JTTEE5 20:1056–1062
DOI: 10.1007/s11666-011-9658-5
1059-9630/$19.00 © ASM International

Effect of Thermal Aging on Microstructure and Mechanical Properties of Plasma-Sprayed Samarium Zirconate Coatings

Jianhua Yu, Huayu Zhao, Xiaming Zhou, Shunyan Tao, and Chuanxian Ding

(Submitted October 2, 2010; in revised form March 31, 2011)

The rare-earth zirconates with the general formula of $Ln_2Zr_2O_7$ (Ln = rare-earth elements) having considerable low thermal conductivity and exhibiting good phase stability at high temperature have attracted particular interest in thermal barrier coating (TBC) applications. The $Sm_2Zr_2O_7$ coatings were deposited by plasma spraying, and the effect of thermal aging on their microstructure and mechanical properties was examined. The lamellar structure gradually disappeared with the temperature increasing for thermal aging. The evaluation by image analysis revealed that the amount of microcrack in coatings decreased with increasing aging temperature because of the increase in aspect ratio caused by microcrack healing, while no obvious change was observed in the spherical porosity. The as-sprayed $Sm_2Zr_2O_7$ coating exhibited low microhardness and elastic modulus, which increased with rise in aging temperature because of the microstructure reconfiguration; in addition, the ratio of microhardness to elastic modulus decreased with aging temperature increase, indicating a promotion in plastic property.

Keywords elastic modulus, microhardness, microstructure, plasma spraying, $Sm_2Zr_2O_7$ coatings

1. Introduction

Thermal barrier coatings (TBCs) based on yttria partially stabilized zirconia (YSZ) have been widely used for thermal protection of hot-sectional metal components in gas turbines (Ref 1, 2). However, the phase transformation and accelerated sintering of coatings result in a reduction of strain tolerance in combination with an increase in Young's modulus as well as a volume change of the coating (Ref 3-5). Great effort is being taken to develop of TBCs materials with low thermal conductivity, high temperature phase stability, and high sintering resistance. Among the numerous oxides that have been explored as TBCs candidate, the pyrochlore-structured rare-earth zirconates—$Ln_2Zr_2O_7$ (Ln-La, Nd, Sm, and Gd)—have attracted particular interest (Ref 6-10). Suresh et al. (Ref 11, 12) have reported that the thermal conductivities of (87-91% dense) pyrochlore-structured $Ln_2Zr_2O_7$ ceramics vary from 1.5 to 1.6 W m^{-1} K^{-1} (at 700 °C). However, the 7 wt.% Y_2O_3-ZrO_2 (7YSZ) ceramics exhibit a thermal conductivity of 3.0 W m^{-1} K^{-1} at room temperature and 2.3 W m^{-1} K^{-1} at 700 °C (Ref 8). Plasma-sprayed $La_2Zr_2O_7$ coatings were performed, and their thermal conductivity is found to be ~0.75 W m^{-1} K^{-1} at 700 °C (Ref 6), which is lower than that of the YSZ coating prepared by plasma spraying. However, the low thermal expansion coefficient and poor fracture toughness of $La_2Zr_2O_7$ coatings contributed to early failure (Ref 7). Wu et al. (Ref 8) reported a thermal conductivity of 1.5 W m^{-1} K^{-1} at 700 °C for hot-pressed $Sm_2Zr_2O_7$ ceramics with a relative density of 98%, which is approximately 30% lower than that of pressless-sintered 7YSZ, while the thermal expansion coefficient and elastic modulus are comparable to those of 7YSZ. Recently, a report showed that thermal conductivity of electron-beam directed-vapor-deposited $Sm_2Zr_2O_7$ coatings is one half that of the 7YSZ coating prepared by the same technology (Ref 13). In our previous study, the thermal conductivity of plasma-sprayed $Sm_2Zr_2O_7$ coating was measured to be 0.38 W m^{-1} K^{-1} at 700 °C, lower than that of YSZ and $La_2Zr_2O_7$ coatings (Ref 6, 14). In addition, YSZ TBCs exposed to high temperatures for extended period in service promote the microstructure reconfiguration, which modifies their mechanical and thermo-physical properties (Ref 15-18). Therefore, an interest has been taken in $Sm_2Zr_2O_7$ coatings. The coatings were deposited by plasma spraying. The microstructure and mechanical properties evolution were explored, and the effect of thermal aging on microstructure and mechanical properties of coatings was discussed.

Jianhua Yu, Huayu Zhao, Xiaming Zhou, Shunyan Tao, and **Chuanxian Ding**, Key Laboratory of Inorganic Coating Materials, Chinese Academy of Sciences, Shanghai 200050, China; **Jianhua Yu, Huayu Zhao, Xiaming Zhou, Shunyan Tao,** and **Chuanxian Ding**, Shanghai Institute of Ceramic, Chinese Academy of Sciences, Shanghai 200050, China; and **Jianhua Yu**, Graduate School of the Chinese Academy of Sciences, Beijing 100039, China. Contact e-mail: shunyantao@mail.sic.ac.cn; yujianhua@mail.sic.ac.cn.

2. Experimental Procedure

$Sm_2Zr_2O_7$ powder was synthesized by a solid-state reaction method. Sm_2O_3 (≥99.9%) and ZrO_2 (≥99.8%) powders were weighted and mixed according to the stoichiometric ratios. After the reaction at 1550 °C, the powder was ground and spray dried, the grain size distribution is mainly in the range of 40-90 μm, with a median size (D50) of ~60 μm. The $Sm_2Zr_2O_7$ coating samples were deposited onto aluminum substrate using the PT-A2000 atmospheric plasma spraying system equipped with an F4-MB plasma gun (Sulzer Metco AG, Wohlen, Switzerland). The plasma spraying parameters are shown in Table 1. The obtained coating samples were debonded from the substrate, then thermal aged at 1200, 1300, 1400, and 1500 °C for 50 h, in a resistance furnace in air.

Microstructure of $Sm_2Zr_2O_7$ coatings was examined using a field emission electron microscope (SEM, JSM 6700F, JEOL, Tokyo, Japan) and an EMPA-8705 QH2 electron probe analyzer (Shimadzu, Tokyo, Japan). The phase compositions of the coatings before and after thermal aging were characterized by x-ray diffraction using a Rigaku D/Max2550 Diffractometer with Cu Kα (λ = 0.15406 nm) radiation at a scan rate of 4° min^{-1}, and the step size is 0.02°. The divergence (DS), scattering (SS), and receiving (RS) slits are 1°, 1°, and 0.3 mm, respectively.

Information on porosity was obtained by image analysis (IA) method. Regarding IA evaluation, the cross section of as-sprayed and thermal-aged $Sm_2Zr_2O_7$ coatings were ground and polished, and five back-scattered electron images (BEIs) with 1000× were taken randomly in each sample for image analysis. The BEIs were converted to binary images to outline pores and cracks, and the total porosity was calculated. As microcracks and pores have different aspect ratios (the ratio of the minor axis over the major axis), defects with a value of aspect ratio below 0.1 were defined as microcracks, while those with an aspect ratio value ranging from 0.1 to 1 were defined as pores.

The Knoop hardness was measured on the cross section of coating samples using an HX-1000 microhardness tester. The measurement was carried out with an indentation load of 2.94 N and a dwell time of 15 s. For examination, a total of 20 indentations were made in randomly located position of each sample. The elastic modulus can be determined by the Knoop indentation using the following equation (Ref 19):

$$\frac{b}{a} = \frac{b'}{a'} - \frac{\alpha H}{E} \qquad \text{(Eq 1)}$$

Table 1 Plasma spraying parameters

Parameters	Value
Arc current, A	600-650
Primary plasma gas Ar, slpm	30-40
Secondary plasma gas H_2, slpm	10-15
Carrier gas Ar, slpm	3.0
Spray distance, mm	120
Nozzle diameter, mm	6.0
Powder inject diameter, mm	2.0

where a and b are the major and minor axes of the measured Knoop indentation after elastic recovery; b'/a' (= 1/7.11) denotes the ratio of the minor to the major dimensions of the ideal Knoop indenter; α is a constant with a value of 0.45; H is the Knoop hardness, and E is the elastic modulus.

3. Results and Discussion

3.1 Phase Stability

Figure 1 shows the XRD patterns of as-sprayed and thermal-aged $Sm_2Zr_2O_7$ coatings. As can be seen from Fig. 1(a), the typical fluorite-type structure $Sm_2Zr_2O_7$ appeared in the as-sprayed coating is in good agreement with the result of EB-DVD coatings (Ref 13), which may be formed because of the high quenching rate (10^6 °C s^{-1}) (Ref 20) of molten $Sm_2Zr_2O_7$ particles during plasma spraying. For the coating that is thermal aged at 1200 °C for 50 h, no obvious change in the crystalline except for the appearance of (331) peak was observed. However, the pyrochlore crystalline phase appeared in the coating aged at 1300 °C for 50 h (Fig. 1c), which is characterized by the presence of the typical supper-lattice peaks at 2θ values of about 37° (331) and 45° (511) using Cu Kα radiation (Ref 21). From Fig. 1(d) and (e), another typical supper-lattice peak of 28° (311) for pyrochlore crystalline phase was observed in the coatings which were thermal aged at 1400 and 1500 °C for 50 h, respectively. However, it is difficult to determine the content of pyrochlore phase because of the overlaps of the main peaks for pyrochlore and fluorite phases. No ZrO_2 diffraction peaks were observed in Fig. 1, which had been earlier observed in the plasma-sprayed $La_2Zr_2O_7$ coatings thermal aged at 1300 °C for 50 h (Ref 6, 10). It is known that the order-disorder transition in rare-earth zirconates is accompanied essentially by no

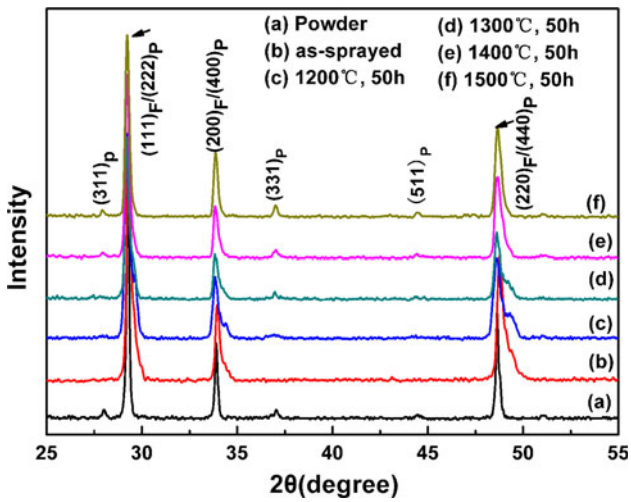

Fig. 1 XRD patterns of as-sprayed and thermal-aged $Sm_2Zr_2O_7$ coatings

volume change (Ref 22), indicating that the phase transformation might have little influence on the thermal cycling performance.

3.2 Microstructure

To observe the grain morphology and lamellar structure in the as-sprayed coating clearly, polished surface and cross section of $Sm_2Zr_2O_7$ coatings were etched by acid solution with 3% hydrochloric acid (AR, Sinopharm Chemical Reagent Co., Ltd.) and 5% hydrofluoric acid (AR, Shanghai Ling-feng Chemical Reagents Limited). Micrograph of the acid-etched surface and cross-sectional $Sm_2Zr_2O_7$ coatings is presented in Fig. 2. Small grains with size of about 200 nm existed in the as-sprayed coatings (Fig. 2a), which formed because of the high quenching rate in plasma spray. Splat boundaries and columnar grains in the as-sprayed $Sm_2Zr_2O_7$ coating are illustrated in Fig. 2(b). The columnar grains arise from directional heat extraction through the substrate and also from the solidification direction (Ref 23).

The fracture surfaces of as-sprayed and thermal-aged $Sm_2Zr_2O_7$ coatings are shown in Fig. 3. The columnar grains in the as-sprayed coating (Fig. 3a) was not obvious even after thermal aging at 1200 °C, which disappeared for the sample aged at 1300 °C for 50 h. This was probably related to the growth of pyrochlore phase in agreement with the XRD result as observed in Fig. 1. Similar phenomenon was observed for lamellar structure, which gradually decreased with increasing aging temperature. The lamellar structure for the as-sprayed $Sm_2Zr_2O_7$ coatings disappeared after aging at 1500 °C for 50 h, and the fracture surface was somewhat similar to that of ceramics.

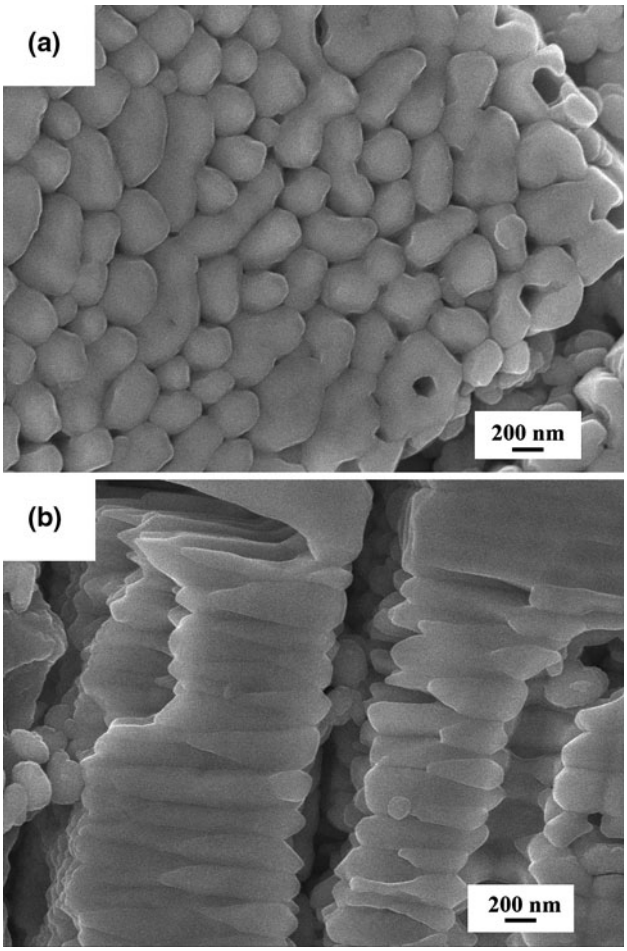

Fig. 2 Acid-etched surface (a) and cross section (b) morphology of as-sprayed $Sm_2Zr_2O_7$ coatings

Figure 4 shows both BEIs and the corresponding binary maps obtained from the BEIs of the as-sprayed and thermal-aged $Sm_2Zr_2O_7$ coatings for 50 h at 1200-1500 °C. Figure 5 represents the characteristic BEIs for the as-sprayed and aged coatings at 1200 and 1500 °C. Distinctive differences are observed in microstructure for the as-sprayed and aged coatings. Directional (horizontal to the splat of coating) microcracks predominating in the as-sprayed coating become not obvious for the aged samples at high temperatures. As observed in Fig. 5(b), narrow microcracks healing occurred by forming necks along the microcracks accompanying with appearance of micropores. However the micropore predominates in the coating aged at 1500 °C (Fig. 5c), indicating that healing of larger defects such as coarse void and microcracks becomes possible at high temperatures. The phenomenon is in good accordance with the observation in Fig. 3.

The total porosity, spherical porosity and amount of crack existed in coatings were estimated using image analysis method, and the result is shown in Fig. 6. The porosity of the as-sprayed $Sm_2Zr_2O_7$ coating was similar to that of the aged coating at 1200 °C for 50 h, although a slight decrease was observed for the coatings aged with further increase in aging temperature. The amount of cracks decreased significantly with increasing aging temperature, which reduced from $4.2 \pm 0.9\%$ in the as-sprayed coating to $2.3 \pm 0.8\%$ in the coating heat treated at 1200 °C, and then to $0.3 \pm 0.2\%$ for the coating aged at 1500 °C, which was in good agreement with the observation in Fig. 4 and 5. The porosity decrease in thermal-aged coatings may be due to the formation of necks along the microcrack, which decreased the length of the microcrack and increased its aspect ratio, and then resulted in decrease in the amount of cracks and total porosity. However, no considerable changes in the spherical porosity was observed for the aged samples at different temperatures, which was higher than that in the as-sprayed coating, suggesting that $Sm_2Zr_2O_7$ coating has good ability to maintain the porous structure.

3.3 Mechanical Properties

It is known that thermal aging is a key factor influencing the mechanical properties of plasma-sprayed deposits. Figure 7 compiles values of Knoop hardness (H) and elastic modulus (E) of the as-sprayed and thermal-aged $Sm_2Zr_2O_7$ coatings. The obtained hardness value for the as-sprayed coating was ~3.1 ± 0.5 GPa, which increased with rise in thermal-aging temperature. As observed in Fig. 2 and 3(a), there are defects, such as

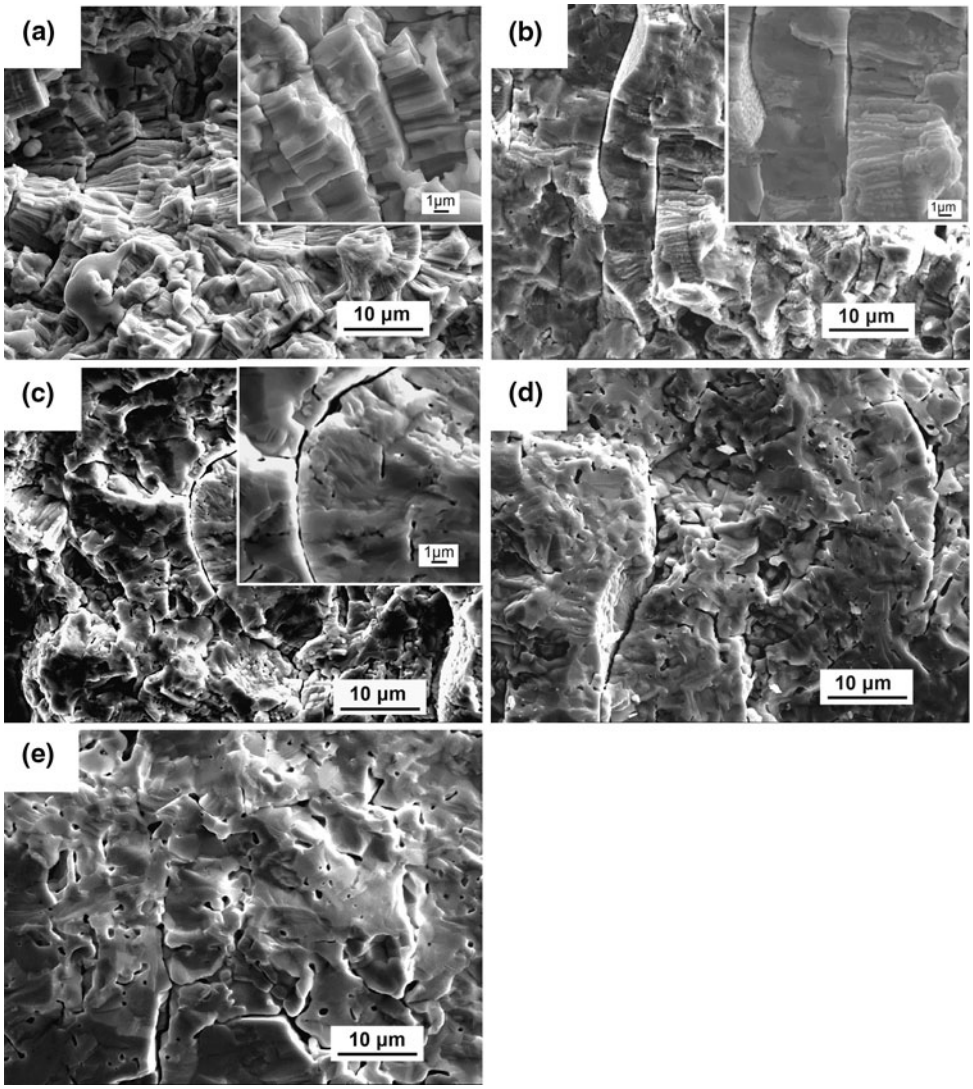

Fig. 3 Fracture surfaces of $Sm_2Zr_2O_7$ coatings as-sprayed (a), thermal aged at 1200 °C (b), 1300 °C (c), 1400 °C (d), and 1500 °C (e) for 50 h

pores and microcracks in the as-sprayed coating, which resulted in a low H value, while the subsequent thermal aging promotes curing of the defects in the samples, resulting in an increase in H value (Ref 15).

The value of elastic modulus for the as-sprayed $Sm_2Zr_2O_7$ coating was only 10% of that reported for the bulk material (231GPa) (Ref 24), which increased significantly after thermal aging. It is known that the reduction in elastic modulus value of thermal-sprayed deposits related not only to the porosity but also to the pore morphology and orientation, and the relationship between E and porosity is given by (Ref 25):

$$E = E_0\left[1 - \left(\frac{5a}{4c} + \frac{3}{4}\right)P\right] \quad \text{(Eq 2)}$$

where E_0 is the elastic modulus of a bulk material; c is the axis that is parallel to the stress direction; a is the axis in the plane that is perpendicular to axis c; and P is the volume of porosity. Materials that contain pores undergo a larger decrease in the elastic modulus value, and the decrease is determined by the orientation and aspect ratio of pores.

The elastic modulus of coating rises significantly under high temperature exposure, because sintering strengthens the bonding between the splats and blocks the sliding along the splat boundaries (Ref 26), moreover grain growth and microcrack healing during thermal aging contributed to improvements in bonding and coherence across the splat boundary as observed in Fig. 3 and 4. This is expected to raise the stiffness appreciably, although the continued presence of the microcracks will ensure that it remains relatively low. The increase in elastic modulus will reduce the strain tolerance, raise the residual stress levels and associated strain energy release rate, making spallation more likely (Ref 15). It is known that the mechanical behavior of materials strongly depends on the combination of its hardness and elastic modulus (Ref 27). The ratio of hardness to elastic modulus (H/E) can be considered as an indicator for the degree of elastic response in

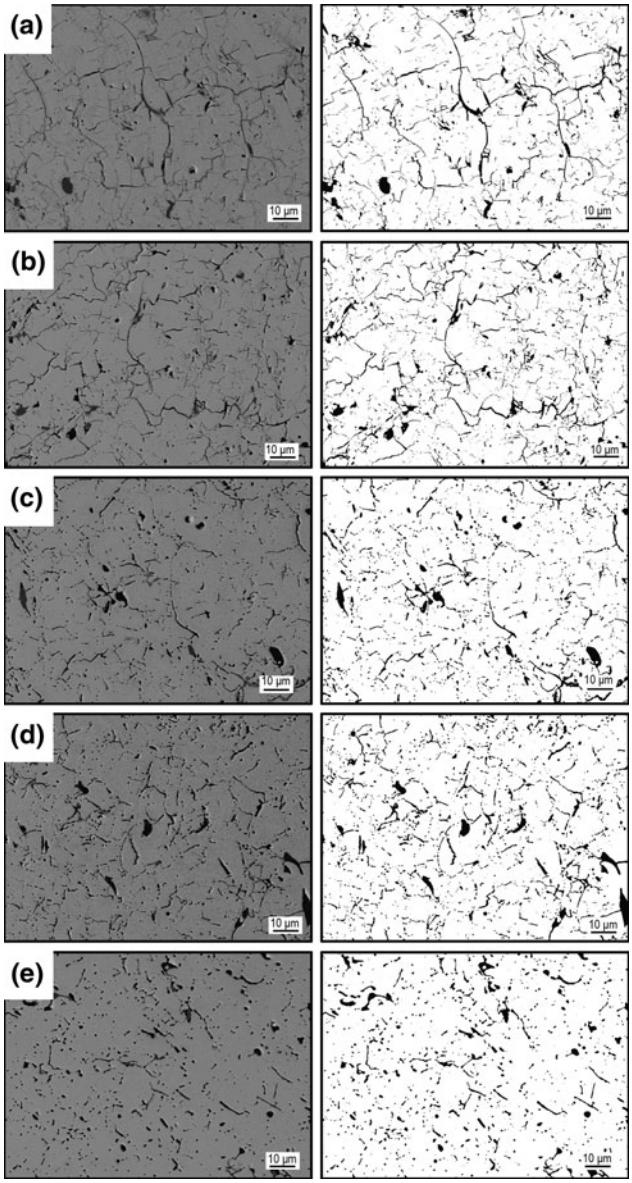

Fig. 4 BEI and binary images of the cross sections for as-sprayed (a) and thermal aged $Sm_2Zr_2O_7$ coatings at 1200 °C (b), 1300 °C (c), 1400 °C (d), and 1500 °C (e) for 50 h

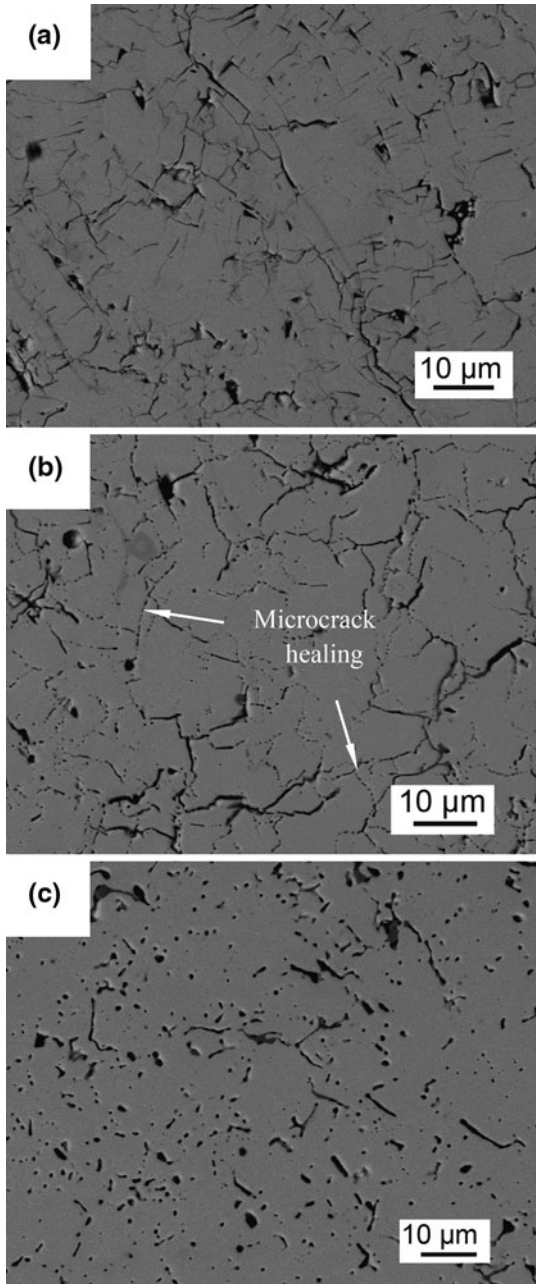

Fig. 5 SEM images of polished cross-sectional as-sprayed (a) and thermal-aged $Sm_2Zr_2O_7$ coatings at 1200 °C (b), and 1500 °C (c) for 50 h

elastic-plastic materials, which is small for rigid/plastic materials and increases for more elastic materials (Ref 28). The value of H/E as shown in Fig. 7 decreased with increase in aging temperature, which suggested that the plasma-sprayed $Sm_2Zr_2O_7$ coatings behave more plastically after thermal aging, as reported for plasma-sprayed Al_2O_3 and ZrO_2 coatings (Ref 28).

4. Conclusions

$Sm_2Zr_2O_7$ coatings were deposited by plasma spraying and thermal aged. Their microstructure and mechanical property were evaluated. Conclusions of this study are summarized as follows:

(1) A typical lamellar structure with columnar grains formed in the as-sprayed $Sm_2Zr_2O_7$ coating, which decreased with increasing aging temperature, and disappeared after aging at 1500 °C for 50 h, because of microcrack healing.

(2) The result of the estimated porosity of $Sm_2Zr_2O_7$ coatings revealed that the formation of necks along a microcrack due to thermal aging resulted in increase

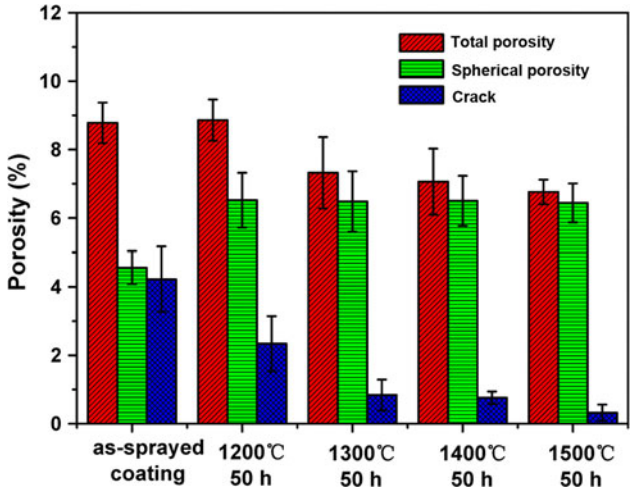

Fig. 6 Total porosity, spherical porosity and amount of crack for coatings before and after thermal aging

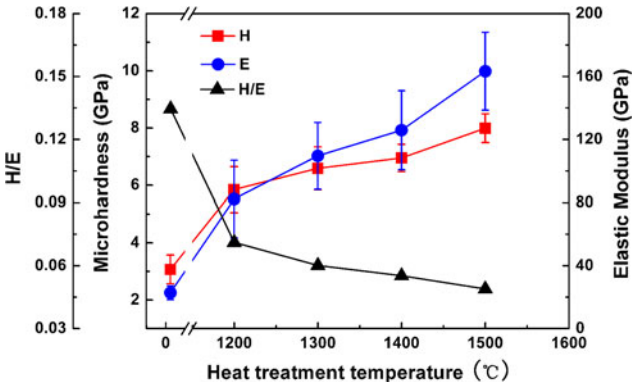

Fig. 7 Hardness, elastic modulus and the ratio of them for $Sm_2Zr_2O_7$ coatings

in defect aspect ratio (the ratio of the minor axis over the major axis), which promoted decrease in porosity, while the spherical pores changed little.

(3) Plasma-sprayed $Sm_2Zr_2O_7$ coatings exhibited low microhardness and elastic modulus because of the existence of pores and microcracks. Both values increased with increasing aging temperature, which is due to the increase in crack aspect ratio and decrease in porosity. However, the decrease in *H*/*E* indicated improved plastic property after thermal aging for $Sm_2Zr_2O_7$ coatings.

Reference

1. N.P. Padture, M. Gell, and E.H. Jordan, Materials Science—Thermal Barrier Coatings for Gas-Turbine Engine Applications, *Science*, 2002, **296**(5566), p 280-284
2. R.A. Miller, Current Status of Thermal Barrier Coatings—An Overview, *Surf. Coat. Technol.*, 1987, **30**(1), p 1-11
3. D.M. Zhu and R.A. Miller, Sintering and Creep Behavior of Plasma-Sprayed Zirconia- and Hafnia-Based Thermal Barrier Coatings, *Surf. Coat. Technol.*, 1998, **109**(1-3), p 114-120
4. D.R. Clarke and C.G. Levi, Materials Design for the Next Generation Thermal Barrier Coatings, *Annu. Rev. Mater. Res.*, 2003, **33**, p 383-417
5. K. An, K.S. Ravichandran, R.E. Dutton, and S.L. Semiatin, Microstructure, Texture, and Thermal Conductivity of Single-Layer and Multilayer Thermal Barrier Coatings of Y_2O_3-Stabilized ZrO_2 and Al_2O_3 Made by Physical Vapor Deposition, *J. Am. Ceram. Soc.*, 1999, **82**(2), p 399-406
6. H.F. Chen, Y.F. Gao, S.Y. Tao, Y. Liu, and H.J. Luo, Thermophysical Properties of Lanthanum Zirconate Coating Prepared by Plasma Spraying and the Influence of Post-Annealing, *J. Alloy Compd.*, 2009, **486**(1-2), p 391-399
7. X.Q. Cao, Application of Rare Earths in Thermal Barrier Coating Materials, *J. Mater. Sci. Technol.*, 2007, **23**(1), p 15-37
8. J. Wu, X.Z. Wei, N.P. Padture, P.G. Klemens, M. Gell, E. Garcia, P. Miranzo, and M.I. Osendi, Low-Thermal-Conductivity Rare-Earth Zirconates for Potential Thermal-Barrier-Coating Applications, *J. Am. Ceram. Soc.*, 2002, **85**(12), p 3031-3035
9. R. Vassen, X.Q. Cao, F. Tietz, D. Basu, and D. Stover, Zirconates as New Materials for Thermal Barrier Coatings, *J. Am. Ceram. Soc.*, 2000, **83**(8), p 2023-2028
10. X.Q. Cao, R. Vassen, W. Jungen, S. Schwartz, F. Tietz, and D. Stover, Thermal Stability of Lanthanum Zirconate Plasma-Sprayed Coating, *J. Am. Ceram. Soc.*, 2001, **84**(9), p 2086-2090
11. G. Suresh, G. Seenivasan, M.V. Krishnaiah, and P.S. Murti, Investigation of the Thermal Conductivity of Selected Compounds of Gadolinium and Lanthanum, *J. Nucl. Mater.*, 1997, **249**(2-3), p 259-261
12. G. Suresh, G. Seenivasan, M.V. Krishnaiah, and P.S. Murti, Investigation of the Thermal Conductivity of Selected Compounds of Lanthanum, Samarium and Europium, *J. Alloy Compd.*, 1998, **269**(1-2), p L9-L12
13. H.B. Zhao, C.G. Levi, and H.N.G. Wadley, Vapor Deposited Samarium Zirconate Thermal Barrier Coatings, *Surf. Coat. Technol.*, 2009, **203**(20-21), p 3157-3167
14. J.H. Yu, H.Y. Zhao, S.Y. Tao, X.M. Zhou, and C.X. Ding, Thermal Conductivity of Plasma Sprayed $Sm_2Zr_2O_7$ Coatings, *J. Eur. Ceram. Soc.*, 2010, **30**(3), p 799-804
15. J.A. Thompson and T.W. Clyne, The Effect of Heat Treatment on the Stiffness of Zirconia Top Coats in Plasma-Sprayed TBCs, *Acta Mater.*, 2001, **49**(9), p 1565-1575
16. F. Cernuschi, P.G. Bison, S. Marinetti, and P. Scardi, Thermophysical, Mechanical and Microstructural Characterization of Aged Free-Standing Plasma-Sprayed Zirconia Coatings, *Acta Mater.*, 2008, **56**(16), p 4477-4488
17. Y. Tan, J.P. Longtin, S. Sampath, and H. Wang, Effect of the Starting Microstructure on the Thermal Properties of As-Sprayed and Thermally Exposed Plasma-Sprayed YSZ Coatings, *J. Am. Ceram. Soc.*, 2009, **92**(3), p 710-716
18. S.R. Choi, D.M. Zhu, and R.A. Miller, Effect of Sintering on Mechanical Properties of Plasma-Sprayed Zirconia-Based Thermal Barrier Coatings, *J. Am. Ceram. Soc.*, 2005, **88**(10), p 2859-2867
19. J.F. Li and C.X. Ding, Determining Microhardness and Elastic Modulus of Plasma-Sprayed Cr_3C_2-NiCr Coatings Using Knoop Indentation Testing, *Surf. Coat. Technol.*, 2001, **135**(2-3), p 229-237
20. R. Mcpherson, A Review of Microstructure and Properties of Plasma Sprayed Ceramic Coatings, *Surf. Coat. Technol.*, 1989, **39**(1-3), p 173-181
21. B.P. Mandal and A.K. Tyagi, Preparation and High Temperature ARD Studies on a Pyrochlore Series with the General Composition Gd_2-*x*Nd*x*Zr_2O_7, *J. Alloy Compd.*, 2007, **437**(1-2), p 260-263
22. M.J.D. Rushton, C.R. Stanek, A.R. Cleave, B.P. Uberuaga, K.E. Sickafus, and R.W. Grimes, Simulation of Defects and Defect Processes in Fluorite and Fluorite Related Oxides: Implications for Radiation Tolerance, *Nucl. Instrum. Meth. B*, 2007, **255**(1), p 151-157
23. S. Sampath and H. Herman, Rapid Solidification and Microstructure Development During Plasma Spray Deposition, *J. Therm. Spray Technol.*, 1996, **5**(4), p 445-456
24. M.P. Vandijk, K.J. Devries, and A.J. Burggraaf, Oxygen Ion and Mixed Conductivity in Compounds with the Fluorite and

Pyrochlore Structure, *Solid State Ionics*, 1983, **9-10**(Dec), p 913-919
25. R.C. Rossi, Prediction of Elastic Moduli of Composites, *J. Am. Ceram. Soc.*, 1968, **51**(8), p 433
26. K.F. Wesling, D.F. Socie, and B. Beardsley, Fatigue of Thick Thermal Barrier Coatings, *J. Am. Ceram. Soc.*, 1994, **77**(7), p 1863-1868
27. J. Musil, F. Kunc, H. Zeman, and H. Polakova, Relationships Between Hardness, Young's Modulus and Elastic Recovery in Hard Nanocomposite Coatings, *Surf. Coat. Technol.*, 2002, **154**(2-3), p 304-313
28. S.H. Leigh, C.K. Lin, and C.C. Berndt, Elastic Response of Thermal Spray Deposits Under Indentation Tests, *J. Am. Ceram. Soc.*, 1997, **80**(8), p 2093-2099